Numerical Methods in Geotechnical Engineering – Benz & Nordal (eds)
© 2010 Taylor & Francis Group, London, ISBN 978-0-415-59239-0

Anisotropic small strain stiffness within the multilaminate framework

B. Schädlich & H.F. Schweiger
Computational Geotechnics Group, Institute for Soil Mechanics and Foundation Engineering, Graz University of Technology, Graz, Austria

ABSTRACT: Using the spectral decomposition of the global compliance matrix, a novel approach to modelling anisotropic elasticity within the multilaminate framework is presented. The new approach is implemented into a soil model which accounts for degradation of small strain stiffness with increasing shear strain and stress dependency of stiffness. The model is calibrated by back-analysis of element tests on London Clay and applied in a Finite Element calculation to evaluate the influence of anisotropic small strain stiffness on deformations connected with tunnel excavation.

1 INTRODUCTION

The high initial elastic stiffness of soils at very small strains ($<10^{-6}$) and its degradation with accumulation of strain is well known since the early 1970ies. With increasing progress in both laboratory testing and soil modelling, taking that effect into account in geotechnical engineering has become more and more common practice within the last decade.

Still, in most practical cases soil is assumed to behave isotropically at very small strains, although laboratory tests on natural soils indicate strongly cross-anisotropic behaviour (Gasparre 2005, Fioravente 2000).

In the following study an approach to model inherently cross-anisotropic elastic material and degradation of small strain stiffness is presented. The model is applied to a tunnelling problem in order to evaluate the effect of initial anisotropy on deformations within the tunnel and at the ground surface.

2 MULTILAMINATE FRAMEWORK

Multilaminate material models are based on the concept that the material behaviour can be formulated on a distinct number of local planes with varying orientation. The stress – strain state varies from plane to plane, resulting in loading induced anisotropy within an intrinsically isotropic material. The global response of the material to a prescribed load is obtained by summation of the contributions of all planes.

The local stress vector $\sigma_{i,loc}$ is obtained by projecting the global stress vector σ_{gl} with the transformation matrix T_i on plane i.

$$\boldsymbol{\sigma}_{i,loc} = (\mathbf{T}_i)^T \cdot \boldsymbol{\sigma}_{gl} \tag{1}$$

The transformation matrix T_i contains the derivatives of the local stress components with respect to the global axes, represented by the direction cosine of the unit vector $n_i^T = (n_{i,1}, n_{i,2}, n_{i,3})$ normal to the plane i and of two unit vectors within the plane, $s_i^T = (s_{i,1}, s_{i,2}, s_{i,3})$ and $t_i^T = (t_{i,1}, t_{i,2}, t_{i,3})$. Vectors n_i, s_i and t_i must form an orthogonal system of local axes, such that $n_i \cdot s_i = 0$, $n_i \cdot t_i = 0$ and $t_i \cdot s_i = 0$.

$$\mathbf{T}_i = \frac{\partial \boldsymbol{\sigma}_{i,loc}}{\partial \boldsymbol{\sigma}_{gl}} \tag{2}$$

The local elastic strains $\varepsilon_{i,loc}$ are calculated as

$$\boldsymbol{\varepsilon}_{i,loc} = \mathbf{C}_{i,loc} \cdot \boldsymbol{\sigma}_{i,loc} . \tag{3}$$

In the case of isotropic linear elastic material, C_{loc} is equal for all planes. For non-linear elasticity (small strain stiffness), C_{loc} depends on the strain history of each plane and therefore differs from plane to plane, resulting in anisotropic global behaviour.

Global strains are obtained by back-transformation and summation of all local strains:

$$\boldsymbol{\varepsilon}_{gl} = 3 \cdot \sum_i \mathbf{T}_i \cdot \boldsymbol{\varepsilon}_{i,loc} \cdot w_i . \tag{4}$$

The factor of 3 in front of the summation can be derived from the principle of virtual work (Bažant & Prat 1988). The weight factors w_i depend on the chosen integration rule. In this study an integration rule based on 2×33 planes (Bažant & Oh 1985) is used.

While local stresses are a projection of the global stress state (static constraint), local strains are in general not the projection of global strains (kinematic constraint) in multilaminate models but they are in so-called microplane models (Bažant & Prat 1988).

3 ANISOTROPIC SMALL STRAIN STIFFNESS MODEL

3.1 *Concept*

In previous multilaminate-type soil models it was postulated, that the local stress state could be represented by 3 components, whose directions coincided with the direction of the vectors n, s and t (Scharinger et al. 2008). That assumption results in a 3×3 local elastic compliance matrix C_{loc} and a 3×6 transformation matrix T. For elasticity it was further assumed, that on local level normal strains are only caused by normal stresses and tangential strains are only caused by tangential stresses. Therefore, C_{loc} was a diagonal matrix with elements outside the main diagonal equal to 0.

For anisotropic material, the aforementioned assumptions can no longer be maintained. Isotropic compression of an anisotropic material results in shear strains on all planes which are not parallel to the global axes, although only normal stresses are obtained on these planes from Equation 1. Anisotropic material behaviour can therefore not be modelled by using a diagonal local compliance matrix.

The spectral decomposition of the global stress vector offers the possibility to obtain local compliance matrices directly. Cross-anisotropic material with a vertical axis of symmetry is considered further on, although the method is also applicable to fully anisotropic material. Only the step-by-step procedure will be demonstrated in this paper. For details on the theoretical background see Theocaris & Sokolis (2000) and Cusatis et al. (2008).

The global compliance matrix C_{gl} of a cross anisotropic elastic material is fully defined by 5 parameters: two elastic moduli E_v and E_h, one independent shear modulus G_{vh}, and two Poisson's ratios, ν_{vh} and ν_{hh}. If written in Kelvin notation, C_{gl} possesses four eigenvalues, $\lambda_1 \ldots \lambda_4$.

$$\lambda_1 = \frac{\nu_{hh}+1}{E_h}. \tag{5a}$$

$$\lambda_2 = \frac{1-\nu_{hh}}{2E_h} + \frac{1}{2E_v} - \sqrt{\left(\frac{1-\nu_{hh}}{2E_h} - \frac{1}{2E_v}\right)^2 + \frac{2\nu_{hv}^2}{E_h^2}} \tag{5b}$$

$$\lambda_3 = \frac{1-\nu_{hh}}{2E_h} + \frac{1}{2E_v} + \sqrt{\left(\frac{1-\nu_{hh}}{2E_h} - \frac{1}{2E_v}\right)^2 + \frac{2\nu_{hv}^2}{E_h^2}} \tag{5c}$$

$$\lambda_4 = \frac{1}{2G_{vh}} \tag{5d}$$

$$\mathbf{C}_{gl,Kelvin} = \begin{pmatrix} \frac{1}{E_h} & \frac{-\nu_{hv}}{E_h} & \frac{-\nu_{hh}}{E_h} & 0 & 0 & 0 \\ \frac{-\nu_{hv}}{E_h} & \frac{1}{E_v} & \frac{-\nu_{hv}}{E_h} & 0 & 0 & 0 \\ \frac{-\nu_{hh}}{E_h} & \frac{-\nu_{hv}}{E_h} & \frac{1}{E_h} & 0 & 0 & 0 \\ 0 & 0 & 0 & \frac{1}{2G_{vh}} & 0 & 0 \\ 0 & 0 & 0 & 0 & \frac{1}{2G_{vh}} & 0 \\ 0 & 0 & 0 & 0 & 0 & \frac{1+\nu_{hh}}{E_h} \end{pmatrix} \tag{6}$$

Using the idempotent matrices $E_1 \ldots E_4$, which are defined by the 4 eigenvectors of C_{gl}, the global stress vector can be split up into its spectral components or stress modes $\sigma_{gl,1} \ldots \sigma_{gl,4}$.

$$\boldsymbol{\sigma}_{gl} = \sum_m \boldsymbol{\sigma}_{gl,m} = \sum_m \left(\mathbf{E}_m \cdot \boldsymbol{\sigma}_{gl}\right) \tag{7}$$

$$\tan 2\omega = \frac{-2\cdot\sqrt{2}\cdot\frac{\nu_{hv}}{E_v}}{\frac{1-\nu_{hh}}{E_h} + \frac{1}{E_v}} \tag{8}$$

$$\mathbf{E}_1 = \begin{pmatrix} 1/2 & 0 & -1/2 & 0 & 0 & 0 \\ 0 & 0 & 0 & 0 & 0 & 0 \\ -1/2 & 0 & 1/2 & 0 & 0 & 0 \\ 0 & 0 & 0 & 0 & 0 & 0 \\ 0 & 0 & 0 & 0 & 0 & 0 \\ 0 & 0 & 0 & 0 & 0 & 1 \end{pmatrix} \tag{9a}$$

$$\mathbf{E}_2 = \begin{pmatrix} \frac{\cos^2\varpi}{2} & \frac{\cos\varpi\sin\varpi}{\sqrt{2}} & \frac{\cos^2\varpi}{2} & 0 & 0 & 0 \\ \frac{\cos\varpi\sin\varpi}{\sqrt{2}} & \sin^2\varpi & \frac{\cos\varpi\sin\varpi}{\sqrt{2}} & 0 & 0 & 0 \\ \frac{\cos^2\varpi}{2} & \frac{\cos\varpi\sin\varpi}{\sqrt{2}} & \frac{\cos^2\varpi}{2} & 0 & 0 & 0 \\ 0 & 0 & 0 & 0 & 0 & 0 \\ 0 & 0 & 0 & 0 & 0 & 0 \\ 0 & 0 & 0 & 0 & 0 & 0 \end{pmatrix} \tag{9b}$$

$$\mathbf{E}_3 = \begin{pmatrix} \frac{\sin^2\varpi}{2} & \frac{\cos\varpi\sin\varpi}{-\sqrt{2}} & \frac{\sin^2\varpi}{2} & 0 & 0 & 0 \\ \frac{\cos\varpi\sin\varpi}{-\sqrt{2}} & \cos^2\varpi & \frac{\cos\varpi\sin\varpi}{-\sqrt{2}} & 0 & 0 & 0 \\ \frac{\sin^2\varpi}{2} & \frac{\cos\varpi\sin\varpi}{-\sqrt{2}} & \frac{\sin^2\varpi}{2} & 0 & 0 & 0 \\ 0 & 0 & 0 & 0 & 0 & 0 \\ 0 & 0 & 0 & 0 & 0 & 0 \\ 0 & 0 & 0 & 0 & 0 & 0 \end{pmatrix} \tag{9c}$$

$$\mathbf{E}_4 = \begin{pmatrix} 0 & 0 & 0 & 0 & 0 & 0 \\ 0 & 0 & 0 & 0 & 0 & 0 \\ 0 & 0 & 0 & 0 & 0 & 0 \\ 0 & 0 & 0 & 1 & 0 & 0 \\ 0 & 0 & 0 & 0 & 1 & 0 \\ 0 & 0 & 0 & 0 & 0 & 0 \end{pmatrix} \tag{9d}$$

Local stress modes $\sigma_{i,loc,m}$ on plane i are obtained by projecting each global stress mode separately using transformation matrices according to Equation 2.

$$\boldsymbol{\sigma}_{i,loc,m} = \mathbf{T}_i^T \cdot \boldsymbol{\sigma}_{gl,m} \tag{10}$$

Local strain modes $\varepsilon_{i,loc,m}$ are calculated by multiplying each local stress mode $\sigma_{i,loc,m}$ separately with the corresponding eigenvalue λ_m (Equ. 11). The sum of all local strain modes yields the local strain vector $\varepsilon_{i,loc}$, and the sum of all local stress modes equals the local stress vector $\sigma_{i,loc}$ (Equ. 12).

$$\boldsymbol{\varepsilon}_{i,loc,m} = \lambda_m \cdot \boldsymbol{\sigma}_{i,loc,m} \tag{11}$$

$$\boldsymbol{\sigma}_{i,loc} = \sum_m \boldsymbol{\sigma}_{i,loc,m} \; ; \qquad \boldsymbol{\varepsilon}_{i,loc} = \sum_m \boldsymbol{\varepsilon}_{i,loc,m} \tag{12}$$

Back transformation to global level and summation of the local strains follows the same procedure as for isotropic material (Equ. 4).

It should be noted, that in this procedure the local stresses depend on global material parameters, while local strains are obtained by multiplying the local stress modes with the scalar eigenvalues. That differs quite substantially from multilaminate models, where local stresses only depend on plane orientation, and all elastic material properties are described by the local compliance matrix $C_{i,loc}$.

However, local compliance matrices can also be derived directly from the global compliance matrix. Combining Equations 7 and 10–12 yields.

$$\boldsymbol{\varepsilon}_{i,loc} = \sum_m \boldsymbol{\lambda}_m \cdot \mathbf{T}_i^T \cdot \mathbf{E}_m \cdot \boldsymbol{\sigma}_{gl} \; . \tag{13}$$

Comparing Equation 13 with Equation 1 and 3, Equation 14 is found.

$$\boldsymbol{\varepsilon}_{i,loc} = \mathbf{C}_{i,loc} \cdot \mathbf{T}_i^T \cdot \boldsymbol{\sigma}_{gl} = \sum_m \boldsymbol{\lambda}_m \cdot \mathbf{T}_i^T \cdot \mathbf{E}_m \cdot \boldsymbol{\sigma}_{gl} \; . \tag{14}$$

As the matrices E_m are of the order 6×6, Equation 13 only has a unique solution if both T_i and $C_{i,loc}$ also are 6×6 matrices. In that case Equation 13 can be transformed to

$$\mathbf{C}_{i,loc} = \mathbf{T}_i^T \cdot \sum_m \boldsymbol{\lambda}_m \cdot \mathbf{E}_m \cdot \left(\mathbf{T}_i^T\right)^{-1} . \tag{15}$$

That means, that the local stress vector is split up into six components. For the present study local stress and strain components on plane i are defined as

$$\boldsymbol{\sigma}_{i,loc} = \begin{pmatrix} \sigma_{i,n,vol} \\ \sigma_{i,n,dev} \\ \tau_{i,s1} \\ \tau_{i,s2} \\ \tau_{i,t1} \\ \tau_{i,t2} \end{pmatrix} ; \; \boldsymbol{\varepsilon}_{i,loc} = \begin{pmatrix} \varepsilon_{i,n,vol} \\ \varepsilon_{i,n,dev} \\ \gamma_{i,s1} \\ \gamma_{i,s2} \\ \gamma_{i,t1} \\ \gamma_{i,t2} \end{pmatrix} \tag{16}$$

with $\sigma_{i,n,vol}$ ... volumetric normal stress, $\sigma_{i,n,dev}$ ... deviatoric normal stress, $\tau_{i,s1}$ and $\tau_{i,t1}$ ... tangential stresses in direction of s and t resulting from global axial stresses, $\tau_{i,s2}$ and $\tau_{i,t2}$ ... tangential stresses in direction of s and t resulting from global shear stresses.

For this split, the transformation matrix of plane i can be written as

$$\mathbf{T}_i = \begin{bmatrix} 1/3 & n_{i,1}^2 - 1/3 & n_{i,1} \cdot s_{i,1} & 0 \\ 1/3 & n_{i,2}^2 - 1/3 & n_{i,2} \cdot s_{i,2} & 0 \\ 1/3 & n_{i,3}^2 - 1/3 & n_{i,3} \cdot s_{i,3} & 0 \\ 0 & 2n_{i,1} \cdot n_{i,2} & 0 & n_{i,1} \cdot s_{i,2} + n_{i,2} \cdot s_{i,1} \\ 0 & 2n_{i,2} \cdot n_{i,3} & 0 & n_{i,3} \cdot s_{i,2} + n_{i,2} \cdot s_{i,3} \\ 0 & n_{i,1} \cdot n_{i,3} & 0 & n_{i,3} \cdot s_{i,1} + n_{i,1} \cdot s_{i,3} \end{bmatrix} \begin{matrix} n_{i,1} \cdot t_{i,1} & 0 \\ n_{i,2} \cdot t_{i,2} & 0 \\ n_{i,3} \cdot t_{i,3} & 0 \\ 0 & n_{i,1} \cdot t_{i,2} + n_{i,2} \cdot t_{i,1} \\ 0 & n_{i,3} \cdot t_{i,2} + n_{i,2} \cdot t_{i,3} \\ 0 & n_{i,3} \cdot t_{i,1} + n_{i,1} \cdot t_{i,3} \end{matrix} \tag{17}$$

$C_{i,loc}$ depends on the plane orientation and contains non-zero off-diagonal elements for general non-isotropic material. In the case of isotropic elastic material, C_{gl} has only two unique eigenvalues (Equ. 18), yielding a diagonal local compliance matrix (Equ. 19).

$$\lambda_1 = \frac{\nu + 1}{E} \; ; \; \lambda_2 = \frac{1 - 2 \cdot \nu}{E} \tag{18}$$

$$\mathbf{C}_{loc,iso} = \begin{bmatrix} \lambda_2 & 0 & 0 & 0 & 0 & 0 \\ 0 & \lambda_1 & 0 & 0 & 0 & 0 \\ 0 & 0 & \lambda_1 & 0 & 0 & 0 \\ 0 & 0 & 0 & \lambda_1 & 0 & 0 \\ 0 & 0 & 0 & 0 & \lambda_1 & 0 \\ 0 & 0 & 0 & 0 & 0 & \lambda_1 \end{bmatrix} \tag{19}$$

Both local stresses and local strains are projections of the corresponding global quantities. Therefore, both the static and the kinematic constraint are fulfilled.

3.2 *Stress dependency of stiffness*

Laboratory test data indicate, that in cross-anisotropic natural soils E_h depends on σ_h and E_v depends on σ_v (Kuwano & Jardine 2002). However, using such an approach in boundary value problems is prone to cause numerical problems at stress free boundaries because high stresses in one direction and stresses close to zero in the other numerically induce extreme ratios of anisotropy in the material, which causes the global stiffness matrix to become almost singular.

In order to avoid such problems, in this study global stiffness parameters E_v, E_h, and G_{vh} are assumed to depend on the mean effective stress p′ only.

$$E_h = E_{h,ref} \cdot \left(\frac{p'}{p_{ref}}\right)^m \; ; \; E_v = E_{v,ref} \cdot \left(\frac{p'}{p_{ref}}\right)^m$$

$$G_{vh} = G_{vh,ref} \cdot \left(\frac{p'}{p_{ref}}\right)^m \tag{20}$$

With that approach a reference local compliance matrix $C_{loc,ref}$ can be established, calculated from

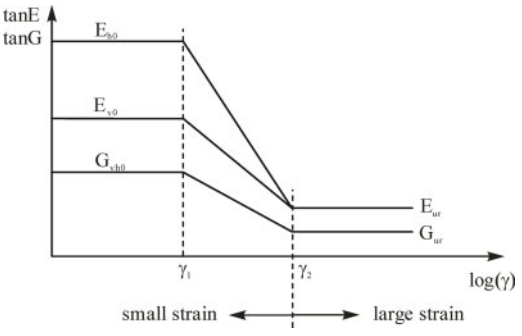

Figure 1. Degradation of anisotropic small strain stiffness.

global stiffness parameters $E_{h,ref}$, $E_{v,ref}$, $G_{vh,ref}$ at the reference pressure p_{ref}. The local compliance matrix at the current stress level is then obtained according to Equation (21).

$$\mathbf{C}_{i,loc} = \mathbf{C}_{i,loc,ref} \cdot \left(\frac{p_{ref}}{p'} \right)^m \tag{21}$$

3.3 *Degradation of stiffness*

Experimental data from laboratory tests show a S-shaped degradation of the initial stiffness with accumulated shear strain (e.g. Gasparre 2005). Various functions describing the degradation of small strain stiffness can be found in the literature, involving trigonometric, exponential and logarithmic functions (e.g. Jardine et al. 1986, Benz 2007).

For the anisotropic multilaminate model, it is assumed that the initially anisotropic material approaches isotropy with increasing accumulated local shear strain γ. Stiffness degradation of E_h follows Equation 22, for the other anisotropic parameters equivalent equations apply. At shear strains larger than γ_2, the material at local level is isotropic, described by the elastic modulus E_{ur} and Poisson's ratio ν_{ur}.

As the development of local shear strains differs from plane to plane, also local stiffness parameters vary over the planes, thus resulting in a smooth transition from small to large strain behaviour on global level. The local shear strains γ_1 and γ_2 have to be determined by back-analysis of laboratory tests.

$$E_h = E_{h0} - (E_{h0} - E_{ur}) \cdot \deg \tag{22}$$

$$\begin{aligned} &\gamma \le \gamma_1 : \deg = 0 \\ &\gamma_1 \le \gamma \le \gamma_2 : \deg = \frac{\log(\gamma) - \log(\gamma_1)}{\log(\gamma_2) - \log(\gamma_1)} \\ &\gamma \ge \gamma_2 : \deg = 1 \end{aligned} \tag{23}$$

3.4 *Plastic strains*

Once the large strain region is reached locally, the model can also account for strain hardening plasticity. As this study is focused on elastic small strain behaviour, the reader is referred to Schweiger et al. (2009) for details on the plasticity part of the model.

Table 1. Elastic soil properties of London Clay.

Parameter	Isotropic	Anisotropic	Unit
$E_{ur,ref}$	13000	13000	kPa
p_{ref}	100	100	kPa
m	1.0	1.0	–
ν_{ur}	0.2	0.2	–
$E_{v0,ref}$	48960	30000	kPa
$E_{h0,ref}$	48960	78000	kPa
$G_{vh0,ref}$	20400	20400	kPa
ν_{hh}	0.2	0.02	–
ν_{vh}	0.2	−0.16	–
γ_1	0.0025	0.0025	%
γ_2	0.03	0.03	%

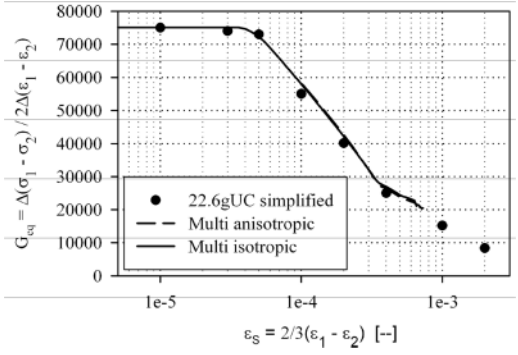

Figure 2. Degradation of equivalent shear modulus.

4 ELEMENT TESTS ON LONDON CLAY

4.1 *Small strain parameters*

Recent experimental data on anisotropic small strain stiffness of London Clay have been published by Gasparre (2005). The samples were retrieved from the site of the Heathrow Terminal 5 and tested using bender element aided triaxial tests. For a depth of 22.6 m, values of $E_{v0} = 110$ Mpa, $E_{h0} = 285$ Mpa, $G_{vh0} = 75$ Mpa, $\nu_{vh} = 0.02$ and $\nu_{hh} = -0.16$ are reported. Reference values at 100 kPa are listed in Table 1. Back analysis of the equivalent shear modulus G_{eq} in undrained triaxial compression tests yielded local shear strains $\gamma_1 = 0.0025\%$ and $\gamma_2 = 0.03\%$ for fitting experimental data (Fig. 2).

However, the same initial shear stiffness G_{eq} and degradation curve could also be obtained assuming isotropic material behaviour (Fig. 2). In that case, G_{eq} would equal the isotropic shear modulus G. Setting $\nu = 0.2$, isotropic values can be derived as $G_{0,ref} = 20.4$ Mpa and $E_{0,ref} = 48.96$ Mpa.

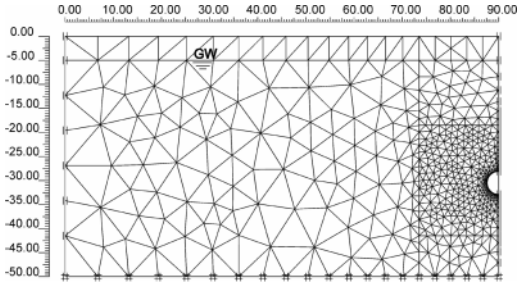

Figure 3. FE-model and boundary conditions.

4.2 *Elastic large strain parameters*

The inclination of the unloading/reloading line in isotropic compression of natural samples is reported as $\kappa = 0.029$ (Gasparre 2005). With $V = 1 + e = 2.12$ (specific volume at reference pressure p_{ref}), $\nu_{ur} = 0.2$ and $p_{ref} = 100\,\text{kPa}$, the unloading reloading stiffness can be obtained as $E_{ur,ref} = 13000\,\text{kPa}$ according to Equation 24.

$$E_{ur,ref} = \frac{3 \cdot (1 - 2\nu_{ur}) \cdot p_{ref}}{\kappa} \cdot (1 + e) \tag{24}$$

5 INFLUENCE OF ANISOTROPIC SMALL STRAIN STIFFNESS

5.1 *FE-model and boundary conditions*

The soil model described above is utilized to investigate the influence of small strain stiffness anisotropy on tunnel induced surface settlements and displacements at the tunnel cross section. The model developed by Scharinger et al. (2008) has been extended to account for anisotropic small strain stiffness. Although the model can also account for plasticity in the large strain range, only elastic strains are considered in this study.

The tunnel centre is situated at 30.5 m depth, diameter of the circular tunnel is 4.75 m. Soil layering is simplified to only one soil layer (Fig. 3).

The calculations are performed with the Finite Element code PLAXIS2D V9.0, using triangular 15-noded elements. Three different sets of soil properties are considered:

- Set 1: no small strain stiffness
- Set 2: isotropic small strain stiffness (Table 1)
- Set 3: anisotropic small strain stiffness (Table 1)

The following boundary conditions are applied in all calculations:

- Ground water table 5 m below ground surface
- $K_0 = 1.5$ (constant over depth)
- Hydrostatic pore water pressure

For simplicity drained conditions are assumed in this study. Starting from the initial stress state, the nodal forces of the tunnel boundary are subsequently reduced from 100% to 0.

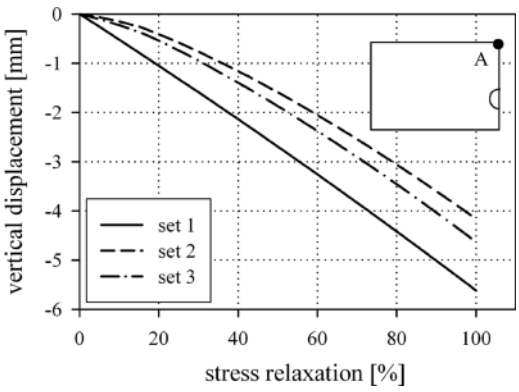

Figure 4. Vertical displacement point A.

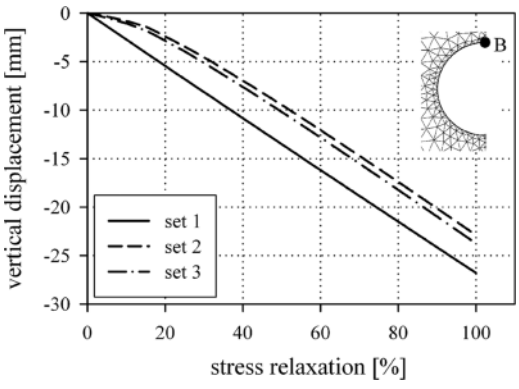

Figure 5. Vertical displacement point B.

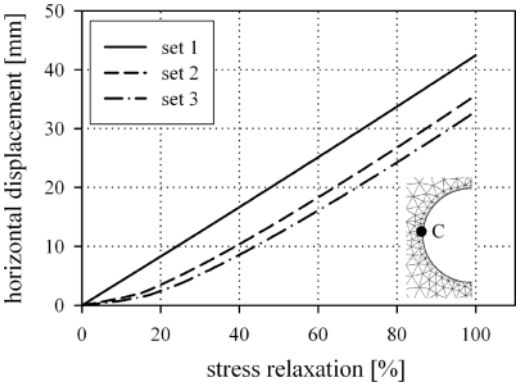

Figure 6. Horizontal displacement point C.

5.2 *Results*

The displacements due to tunnel excavation are compared at the following points:

- Point A – at ground surface above tunnel
- Point B – at tunnel crown
- Point C – at tunnel bench

The development of vertical and horizontal displacements with reduction of initial nodal forces within the tunnel is summarized in Figures 4–6.

Table 2. Displacements [mm] at 40% stress relaxation.

	set 1	set 2	set 3	set 3 / set 2
Point A – u_v	−2.1	−1.2	−1.4	120%
Point B – u_v	−10.8	−7.0	−7.6	109%
Point C – u_h	16.7	10.4	8.6	83%

The curves for point B and C become parallel at 40–50% excavation, indicating the complete loss of small strain stiffness within the soil volume relevant to these points. For point A slightly different inclinations can be found even at full relaxation. The ratio

$$f_{u,aniso} = \frac{u_{aniso}}{u_{iso}} = \frac{u_{set3}}{u_{set2}} \tag{25}$$

at 40% stress relaxation varies from 83% to 120% (Table 2). Although $f_{u,aniso}$ follows the ratio of isotropic vs. anisotropic stiffness (with u_v being governed by $1/E_v$ and u_h by $1/E_h$), the stiffness ratio is considerably higher than $f_{u,aniso}$ (E_{v0} / $E_{iso} = 61\%$; E_{h0} / $E_{iso} = 160\%$).

6 CONCLUSION

A new approach for modelling anisotropic, stress - dependent small strain stiffness within the multilaminate framework has been developed. The stress dependency of stiffness currently implemented in the model does not fully agree with experimentally observed soil behaviour and requires further investigation. Regarding the influence of anisotropy in the small strain range on practical boundary value problems, the study must be seen as preliminary. Only one set of anisotropic parameters was used, and only elastic deformations in a tunnelling problem were considered. However, in the case investigated isotropic and anisotropic small strain stiffness result in similar displacements, if both sets of parameters fit the degradation curve of the equivalent shear modulus G_{eq}. Whether this is a general trend or just coincidence needs to be investigated with more sets of parameters and also in different boundary value problems.

REFERENCES

Addenbrooke, T.I., Potts, D.M. & Puzrin, A.M. 1997. The influence of pre-failure soil stiffness on the numerical analysis of tunnel construction. *Geotechnique* 47 (3): 693–712.

Bažant, Z.P. & Oh, B.H. 1986. Efficient Numerical Integration on the Surface of a Sphere. *Zeitschrift für angewandte Mathematik und Mechanik* 66: 37–49.

Bažant, Z.P. & Prat, P.C. 1988. Microplane Model for Brittle-Plastic Material: I. Theory. *Journal of Engineering Mechanics* 114(10): 1672–1688.

Benz, T. 2007. Small Strain Stiffness of Soils and its Numerical Consequences. Ph.D. Thesis. *Mitteilung 55 des Instituts für Geotechnik*, Universität Stuttgart.

Cusatis, G., Beghini, A. & Bažant, Z.P. 2008. Spectral Stiffness Microplane Model for Quasibrittle Laminates – Part I: Theory. *Journal of Applied Mechanics* 75(2): (021009) 1–9.

Fioravante, F. 2000. Anisotropy of small strain stiffness of Ticino and Kenya sands from seismic wave propagation measured in triaxial testing. *Soils and Foundations* 40(4): 129–142.

Gasparre, A. 2005. Advanced laboratory characterisation of London Clay. PhD thesis, Imperial College, London.

Jardine, R.J., Potts, D.M., Fourie, A.B. & Burland, J.B. 1986. Studies of the influence of non-linear stress-strain characteristics in soil-structure interaction. *Geotechnique* 36 (3): 377–396.

Kuwano, R. & Jardine, R.J. 2002. On the applicability of cross-anisotropic elasticity to granular materials at very small strains. *Geotechnique* 52 (10): 727–749.

Scharinger, F., Schweiger, H.F. & Pande, G.N. 2008. On a multilaminate model for soil incorporating small strain stiffness. *International Journal for Numerical and Analytical Methods in Geomechanics* 33(2): 215–243.

Schweiger, H.F., Wiltafsky, C., Scharinger, F. & Galavi, V. 2009. A multilaminate framework for modelling induced and inherent anisotropy of soils. *Geotechnique* 59 (2): 87–101.

Theocaris, P.S. & Sokolis, D.P. 2000. Spectral decomposition of the compliance fourth-rank tensor for orthotropic materials. *Archive of Applied Mechanics* 70(4): 289–306.